Relationship between thermoelectric figure of merit and energy conversion efficiency

Hee Seok Kim[a], Weishu Liu[a], Gang Chen[b,1], Ching-Wu Chu[a,c,1], and Zhifeng Ren[a,1]

[a]Department of Physics and Texas Center for Superconductivity, University of Houston, Houston, TX 77204-5002; [b]Department of Mechanical Engineering, Massachusetts Institute of Technology, Cambridge, MA 02139; and [c]Lawrence Berkeley National Laboratory, Berkeley, CA 94720

Contributed by Ching-Wu Chu, May 29, 2015 (sent for review April 27, 2015; reviewed by Baowen Li)

The formula for maximum efficiency (η_{max}) of heat conversion into electricity by a thermoelectric device in terms of the dimensionless figure of merit (*ZT*) has been widely used to assess the desirability of thermoelectric materials for devices. Unfortunately, the η_{max} values vary greatly depending on how the average *ZT* values are used, raising questions about the applicability of *ZT* in the case of a large temperature difference between the hot and cold sides due to the neglect of the temperature dependences of the material properties that affect *ZT*. To avoid the complex numerical simulation that gives accurate efficiency, we have defined an engineering dimensionless figure of merit $(ZT)_{eng}$ and an engineering power factor $(PF)_{eng}$ as functions of the temperature difference between the cold and hot sides to predict reliably and accurately the practical conversion efficiency and output power, respectively, overcoming the reporting of unrealistic efficiency using average *ZT* values.

thermoelectrics | engineering figure of merit | engineering power factor | conversion efficiency | cumulative temperature dependence

A thermoelectric (TE) generator produces electric power directly from a temperature gradient through TE material (1–4). The maximum efficiency of a TE generator was first derived based on a constant property model by Altenkirch (5) in 1909, and its optimized formula has been commonly used since Ioffe (6) reported the optimum condition for the maximum efficiency in 1957, which is (7)

$$\eta_{max} = \frac{\Delta T}{T_h} \frac{\sqrt{1+Z\cdot T_{avg}}-1}{\sqrt{1+Z\cdot T_{avg}}+\frac{T_c}{T_h}}, \quad [1]$$

where T_h and T_c are the hot- and cold-side temperatures, respectively, and ΔT and T_{avg} are their difference, $T_h - T_c$, and average $(T_h + T_c)/2$, respectively. The TE conversion efficiency by Eq. **1** is the product of the Carnot efficiency $(\Delta T/T_h)$ and a reduction factor as a function of the material's figure of merit $Z = S^2 \rho^{-1}\kappa^{-1}$, where S, ρ, and κ are the Seebeck coefficient, electrical resistivity, and thermal conductivity, respectively. Since the 1950s, the dimensionless figure of merit (ZT), such as the peak ZT (8–10) and the average ZT (2, 11, 12), has been used as the guide to achieve better materials for higher conversion efficiency.

The maximum efficiency by Eq. **1** is inadequate when Z is temperature dependent. Due to the assumption of temperature independence, Eq. **1** only correctly predicts the maximum efficiency at a small temperature difference between the cold and hot sides, or in limited TE materials (13–15) that have Z almost constant over the whole temperature range. By ignoring the assumption and simply using Eq. **1**, incorrect efficiency that is much higher than is practically achievable (16, 17) is often reported. In most cases for S, ρ, and κ that are temperature dependent, ZT values are not linearly temperature dependent (18–22) and they operate at a large temperature difference, so the prediction by Eq. **1** cannot be reliable. To overcome the inadequacy, complicated numerical simulations based on the finite difference method were carried out to calculate the efficiency while accounting for the temperature dependence over a large temperature difference between the cold and hot sides (23–25). The efficiency by Eq. **1** is conventionally used by getting average Z in two ways: (*i*) an integration with respect to temperature, $Z_{int} = (1/\Delta T)\int_{T_c}^{T_h} Z(T)dT$, and (*ii*) a Z value corresponding to the average temperature, $Z_{T_{avg}} = Z(T_{avg})$. The $Z_{int}T_{avg}$ and $Z_{T_{avg}}T_{avg}$ are called the average ZT hereafter. Fig. 1*A* shows the temperature-dependent ZT and average ZTs of the p-type Ni-doped MgAgSb (26), and their corresponding efficiency calculations by Eq. **1** are shown in Fig. 1*B* and are matched with the numerical simulation of an ideal case because the Z vs. T is not too much off a constant (Fig. S1*A*). In Fig. 1*C*, however, n-type In_4Se_{3-x} (17) has larger variations of average ZTs depending on the method used due to the strong temperature dependence (Fig. S1*B*) resulting in much different efficiency predictions (Fig. 1*D*). Even though the peak ZT of In_4Se_{3-x} is higher than that of Ni-doped MgAgSb, the average ZTs and predicted efficiency are much lower, which means that peak ZT value is not the right indicator for a TE material's efficiency. In addition, any average ZT cannot be a correct index due to lack of consistency for the following reasons: (*i*) average ZTs vary by the averaging techniques (Fig. 1 *A* and *C*), (*ii*) $Z_{T_{avg}}$ is estimated larger than Z_{int} when the Z curve is in convex upward shape (Fig. S1*A*) and vice versa (Fig. S1*B*), and (*iii*) analytical prediction of some materials based on the average ZTs is far away from the numerical analysis (Fig. 1*D*).

As discussed, conventional methods using average ZTs often do not predict a realistic efficiency in practical operating conditions over a large temperature difference between the cold and hot sides because Z is strongly temperature dependent in some materials. Therefore, the conventional efficiency formula (Eq. **1**) often misleads and gives rise to an impractically high efficiency prediction. For this reason, it is desirable to establish a new model to predict the energy conversion efficiency based on the temperature-dependent individual TE properties for devices operating under a large temperature difference. Here, we define an engineering

Significance

Thermoelectric materials generate electricity from temperature gradients. The dimensionless figure of merit, $ZT = S^2\rho^{-1}\kappa^{-1}T$, is calculated from the Seebeck coefficient (*S*), electrical resistivity (ρ), and thermal conductivity (κ). The calculated efficiency based on *ZT* using the conventional formula is not reliable in some cases due to the assumption of temperature-independent *S*, ρ, and κ. We established a new efficiency formula by introducing an engineering figure of merit $(ZT)_{eng}$ and an engineering power factor $(PF)_{eng}$ to predict reliably and accurately the efficiency of materials at a large temperature difference between the hot and cold sides, unlike the conventional *ZT* and *PF* providing performance only at specific temperatures. These new formulas will profoundly impact the search for new thermoelectric materials.

Author contributions: H.S.K. and Z.R. designed research; H.S.K. performed research; H.S.K., W.L., G.C., C.-W.C., and Z.R. analyzed data; H.S.K., W.L., G.C., C.-W.C., and Z.R. wrote the paper.

Reviewers included: B.L., National University of Singapore.

The authors declare no conflict of interest.

[1]To whom correspondence may be addressed. Email: gchen2@mit.edu, cwchu@uh.edu, or zren@uh.edu.

This article contains supporting information online at www.pnas.org/lookup/suppl/doi:10.1073/pnas.1510231112/-/DCSupplemental.

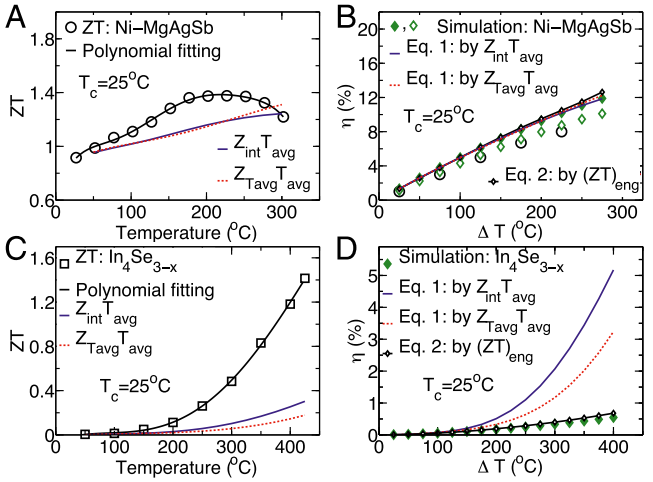

Fig. 1. Inadequacy of the relationship between the conventional *ZT* and the maximum efficiency. (*A*) *ZT* vs. *T* of Ni-doped MgAgSb (26). Circles are measured data, and the black line is the fitted curve. Solid blue and dashed red lines are average *ZT*s by $Z_{int}T_{avg}$ and $Z_{T_{avg}}T_{avg}$, respectively. (*B*) Efficiencies at $T_c = 25$ °C by experimental measurement (circles), by numerical simulation of ideal (solid diamonds) and actual (open diamonds) conditions, by conventional formula using integration (solid blue line) and average temperature (dashed red line) for Z_{avg}, and by the new formula (open squares in black line). The ideal and actual conditions of the numerical predictions denote the cases excluding and including electric contact/parasitic resistance (a total 36 μΩ cm^2 from two ends) (26), respectively. (*C*) *ZT*s vs. *T* and (*D*) efficiencies at $T_c = 25$ °C of In_4Se_{3-x}. The *x* axis in *A* and *C* indicates the hot-side temperature for the averaged *ZT*s, and the measurement temperature for *ZT* data and their polynomial fittings.

dimensionless figure of merit $(ZT)_{eng}$ and an engineering power factor $(PF)_{eng}$ as realistic indicators associated with temperature difference whereas the conventional *ZT* and *PF* indicate a material's performance only at a specific temperature. Based on $(ZT)_{eng}$ and $(PF)_{eng}$, we report the formulas for more accurate prediction of maximum efficiency by accounting for a cumulative temperature dependence of *S*, ρ, and κ regarding a single homogeneous TE material. A generic formula including Thomson heat is also derived with the corrected contribution of Joule and Thomson heat and is applicable to any situation, no matter whether the properties are constant or strongly temperature dependent. This work demonstrates the impact of the $(ZT)_{eng}$ based on the cumulative temperature-dependent properties over the conventional *ZT*.

Results and Discussion

The Formulas by Cumulative Temperature-Dependent Properties. The formula for the maximum efficiency based on cumulative temperature-dependent properties is derived as (see *SI Derivation of the Maximum Efficiency Without Thomson Heat* for a detailed derivation)

$$\eta_{max} = \eta_c \frac{\sqrt{1+(ZT)_{eng}(\hat{\alpha}/\eta_c - 1/2)} - 1}{\hat{\alpha}\left(\sqrt{1+(ZT)_{eng}(\hat{\alpha}/\eta_c - 1/2)} + 1\right) - \eta_c}, \quad [2]$$

where η_c is Carnot efficiency and $(ZT)_{eng}$ is the engineering dimensionless figure of merit defined as

$$(ZT)_{eng} = Z_{eng}\Delta T = \frac{\left(\int_{T_c}^{T_h} S(T)dT\right)^2}{\int_{T_c}^{T_h}\rho(T)dT \int_{T_c}^{T_h}\kappa(T)dT}\Delta T = \frac{(PF)_{eng}}{\int_{T_c}^{T_h}\kappa(T)dT}\Delta T. \quad [3]$$

Z_{eng} is the engineering figure of merit in K^{-1}, $(PF)_{eng}$ is the engineering power factor in W m^{-1}K^{-1}, and $\hat{\alpha}$ is a dimensionless intensity factor of the Thomson effect defined as $\hat{\alpha} = S(T_h)\Delta T / \int_{T_c}^{T_h} S(T)dT$, where $S(T_h)$ is the Seebeck coefficient at the hot-side temperature T_h. The first term of the numerator in Eq. **2** is the optimized ratio of external (R_L) to internal electric resistance (R) for the maximum efficiency. According to Eq. **2**, the maximum efficiencies of Ni-doped MgAgSb and In_4Se_{3-x} are compared with those by Eq. **1** in Fig. 1 *B* and *D*, respectively, in which the efficiency of In_4Se_{3-x} by Eq. **2** based on $(ZT)_{eng}$ is much reduced but in good agreement with the result by numerical simulation. Eqs. **2** and **3** enable one to analytically predict the maximum efficiency more accurately without carrying out numerical simulations nor experimental setup and measurements. $(ZT)_{eng}$, rather than *ZT*, predicts the practical performance of a TE material at any given temperature difference; $\hat{\alpha}$ implies a level of contribution of the Thomson effect to the analytical prediction of the maximum efficiency. The rationale for why Eq. **2** still leads to some overestimation will be discussed later.

Efficiency. The peak *ZT*s of half-Heusler (HH: $Hf_{0.19}Zr_{0.76}Ti_{0.05}CoSb_{0.8}Sn_{0.2}$) (13) and SnSe (22) are 0.94 at 700 °C and 2.6 at 650 °C, respectively, as shown in Fig. 2*A*. The temperature-dependent average *ZT*s of HH calculated by the two methods are almost identical over the whole temperature range whereas those of SnSe differ significantly after $\Delta T = 250$ °C due to the strong temperature dependence of the TE properties (Fig. S2), and the average *ZT*s of SnSe become similar to or much higher than those of HH at $T_h = 700$ °C depending on the averaging technique (Fig. 2*B*). Based on the peak and average *ZT*, one may expect that SnSe gives rise to a much higher efficiency than HH at $\Delta T = 600$ °C and $T_c = 100$ °C when using the conventional formula, Eq. **1**. However, Eq. **2** yields efficiencies of 9.7% for HH and 7.3% for SnSe (Fig. 2*C*), which is opposite to what was expected from Eq. **1** by average *ZT*s (Fig. 2 *D* and *E*). To validate the new efficiency formula compared with the conventional one, a numerical simulation based on a finite difference model (27, 28) was carried out as shown in Fig. 2*C*. The conventional formula overestimates the efficiency of SnSe by a factor of 2, but the new formula we present here predicts more accurate efficiency, overestimated only by 17% compared with the numerical results (Fig. 2 *C* and *E*), which strongly indicates that Eq. **2** should be used in the future to calculate the efficiency of any TE materials using the measured TE properties. In addition, the optimized ratio m_{opt} $(=\sqrt{1+Z\cdot T_{avg}})$ (Eq. **1**) based on averaged *ZT*s for SnSe has large variation with temperature (Fig. S3), where *m* is defined as the ratio of external electric load R_L and internal resistance *R*. Obtaining the correct m_{opt} is essential to design a TE generator and integrate it into applications.

Intensity Factor of Thomson Effect. In Fig. 2*C*, the efficiency of SnSe by Eq. **2** is still overestimated by 17% in comparison with that from numerical simulation whereas that for HH agrees very well with the numerical results. The difference is mainly caused by the lack of Thomson effect on the input heat flux in Eq. **2** whereas the numerical simulations take it into account. However, the relative degree of the Thomson effect contribution to the analytically predicted efficiency can be estimated by $\hat{\alpha}$. Note that $\hat{\alpha} = 1$ when the Seebeck coefficient is temperature independent. If the temperature-dependent Seebeck coefficient follows a monotonic curve, $\hat{\alpha} > 1$ at a given temperature boundary implies $d|S|/dT > 0$, in which the Thomson effect plays a role in increasing the efficiency (29). The magnitude of $\hat{\alpha}$ shows the level of the Thomson effect associated with the temperature difference, which means that one can presume the error of efficiency prediction caused by the absence of Thomson effect in Eq. **2**, where larger $|\hat{\alpha}|$ indicates larger effect of Thomson heat leading to larger error. In Fig. 2*F*, the temperature-dependent $\hat{\alpha}$ of SnSe showing a steep drop below 1 gives rise to the larger gap between the numerical and analytical results, and indicates that the analytical result is overestimated compared with numerical simulation. In contrast, due to smaller $|\hat{\alpha}|$, less Thomson effect comes into play for HH, and $\hat{\alpha}$ above 1 represents the underrated efficiency by Eq. **2** rather than by numerical

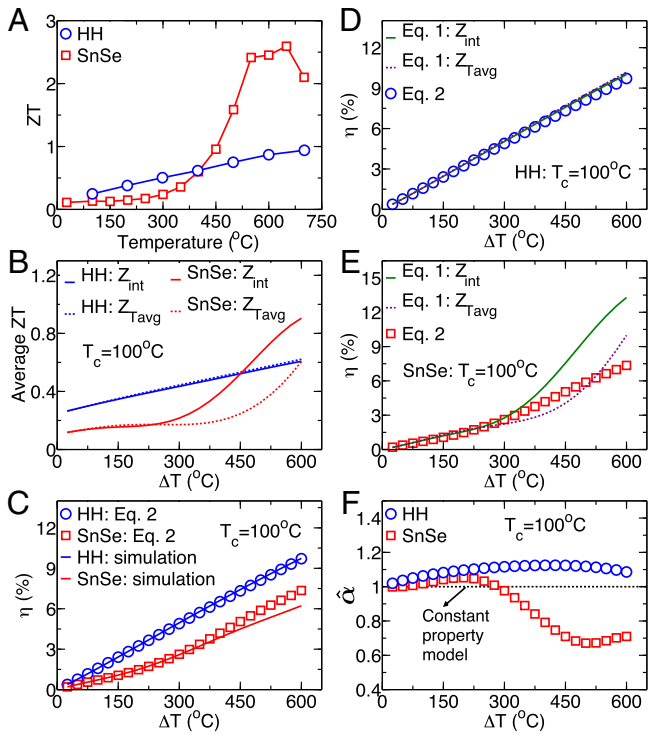

Fig. 2. Analysis of practical efficiency predictions based on cumulative temperature-dependent properties and $(ZT)_{eng}$. (*A*) *ZT* of HH (13) and SnSe (22), where the *x* axis indicates the measurement temperature for thermoelectric transport properties. (*B*) Temperature-dependent average *ZT*s of HH and SnSe based on two methods of averaging techniques. (*C*) Efficiency calculated by Eq. **2** compared with the numerical simulation. (*D*) Maximum efficiency for HH predicted by Eq. **1** and Eq. **2**. (*E*) Maximum efficiency for SnSe predicted by Eq. **1** and Eq. **2**. (*F*) The ΔT-dependent intensity factor of Thomson effect $\hat{\alpha}$ of HH and SnSe, respectively.

analysis. Even though Eq. **2** does not take Thomson effect on the input heat flux into account for the efficiency prediction, it provides which direction as well as how much higher or lower the efficiency is shifted by the cumulative effect of Thomson heat compared with an accurate result.

Engineering Dimensionless Figure of Merit $(ZT)_{eng}$. By revisiting Eqs. **S5** and **S11**, it is noted that the efficiency formula is a strong function of $(ZT)_{eng}$, so the maximized $(ZT)_{eng}$ is highly desired for the maximum efficiency. Fig. 3*A* shows ΔT-dependent $(ZT)_{eng}$ curves of HH and SnSe that have the same trends as the practical efficiency predictions (Fig. 2*C*) through the whole temperature range, in which $(ZT)_{eng}$ implies the equivalent *ZT* at a given ΔT no matter how high the peak *ZT* is. Even though the peak *ZT* of SnSe is much higher than that of HH (Fig. 2*A*), by a factor of 3, the $(ZT)_{eng}$ of SnSe is much lower (Fig. 3*A*). This is because the $(ZT)_{eng}$ is ΔT-dependent whereas *ZT* lacks both effects of the temperature boundary condition and its cumulative effect. To overcome the inadequacy of *ZT*, the effective figure of merit $(ZT)_{eff} = (\int_{T_c}^{T_h} S(T)dT)^2 T_{avg}/(\Delta T \int_{T_c}^{T_h} \rho(T)\kappa(T)dT)$ has been reported (30, 31), of which HH and SnSe is shown as solid lines in Fig. 3*A*, where $(ZT)_{eff}$ also has a tendency somewhat similar to the efficiency excursion rather than average *ZT*s. However, $(ZT)_{eff}$ has impractically large values at very small ΔT, and becomes comparable to $(ZT)_{eng}$ at higher T_h. This indicates that $(ZT)_{eff}$ implies the averaged performance whereas $(ZT)_{eng}$ directly delineates the accumulated performance associated with a given temperature difference. In addition, $(ZT)_{eng}$ shows a better fitted trend with the efficiency prediction as shown in Fig. 3 *B* and *C*, in which the vertical axes represent normalized quantities such as η (open symbols), $(ZT)_{eng}$ (solid lines), and $(ZT)_{eff}$ (dashed lines).

Engineering Power Factor and Output Power Density. The output power density W m^{-2} at the maximum efficiency based on the $(PF)_{eng}$ is expressed as

$$P_d = \frac{(PF)_{eng}\Delta T}{L}\frac{m_{opt}}{(1+m_{opt})^2}. \quad [4]$$

The output power density is dependent on the TE leg's dimensions as well as the material properties whereas the efficiency is determined only by the material's characteristics. Fig. 3 *D* and *E* shows the output power densities of HH and SnSe at T_c = 100 °C with ΔT, where a cubic-shaped TE leg is assumed for the output power prediction, and a simple averaged Seebeck coefficient and electrical resistance at a given temperature difference are used for the conventional *PF*-based prediction. The power density based on $(PF)_{eng}$ has better agreement with the numerical prediction within 1% and 13% of relative difference for HH and SnSe, respectively, whereas that based on conventional *PF* shows 13% and 33% of relative difference at ΔT = 600 °C for HH and SnSe, respectively. The amount of power generation by HH is more than tenfold as large as that of SnSe in the same TE leg dimensions as shown in Fig. 3 *D* and *E* due to the large difference of thermal conductivity of the materials. By adjusting leg dimensions for matching similar input heat range to keep the same ΔT, the power density can be comparable (Fig. S4), but reducing or increasing a leg length causes thermomechanical structural issues that are outside the scope of this study, so the same dimension of leg is considered to examine the intrinsic characteristics of materials for power generation. In Fig. 3*F*, $(PF)_{eng}$ shows similar tendency and relative scale to the power

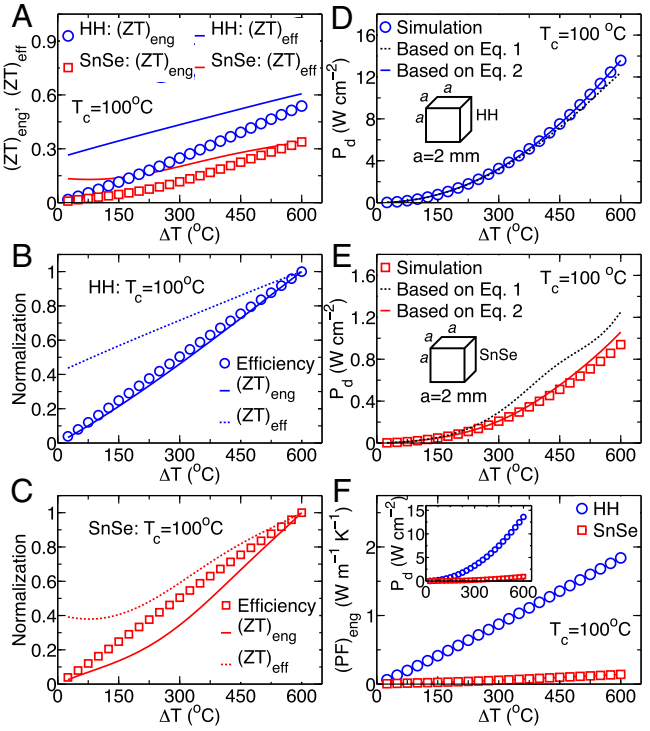

Fig. 3. $(ZT)_{eng}$ and $(PF)_{eng}$ as practical indicators for TE energy conversion efficiency and output power generation, respectively. (*A*) ΔT-dependent $(ZT)_{eng}$ and average-temperature-based $(ZT)_{eff}$. Normalized efficiency by Eq. **2**, normalized $(ZT)_{eng}$, and normalized $(ZT)_{eff}$ for HH (*B*) and for SnSe (*C*). Output power densities of (*D*) HH and (*E*) SnSe with ΔT in a cubic-shaped TE leg. (*F*) ΔT-dependent $(PF)_{eng}$ of HH and SnSe at T_c = 100 °C showing the same tendency as the power density curves (*Inset*).

density by the numerical simulation (Fig. 3*F*, *Inset*), indicating an intrinsic performance for power generation of a TE material operated at practical temperature gradients, which has quite different trends from *PF* (Fig. S2*E*). Thus $(ZT)_{eng}$ and $(PF)_{eng}$ enable one to compare directly the level of a material's performance at any operating temperature differences without the detailed calculations of efficiency and output power generation.

Application to Other TE Materials. Fig. 4 shows the generalization of this work by applying Eqs. **2**–**4** to other TE materials with MgAgSb (26) and HH (13) shown for comparison. At low temperatures up to 300 °C, MgAgSb has higher *ZT* (Fig. 4*A*), average *ZT* (Fig. 4*B*), and $(ZT)_{eng}$ (Fig. 4*C*) among others, which leads to higher conversion efficiency in this temperature range (Fig. 4*D*). Even though the peak *ZT* and average *ZT* of $K_{0.02}Pb_{0.98}Te_{0.75}Se_{0.25}$ (K-PbTeSe) (21) are higher than those of $Ce_{0.45}Nd_{0.45}Fe_{3.5}Co_{0.5}Sb_{12}$ (SKU) (14) by up to 40% of relative difference at $\Delta T = 550$ °C (Fig. 4 *A* and *B*), Eq. **2** and numerical simulation show that their efficiencies are comparable to each other within 8% and 4.5% of relative difference, respectively, whereas Eq. **1** yields the efficiency of K-PbTeSe at 12% relatively higher than that of SKU (Fig. 4*D*). This practical trend of the efficiency by Eq. **2** is simply inferred from $(ZT)_{eng}$, which is more analogous than average *ZT*s. The efficiency of MgAgSb by Eq. **1** shows somewhat better agreement with the numerical simulation than by Eq. **2**. However, there is no analogy to predict quantitatively the difference, and the tendency is not predictable either, i.e., what leads to over- or underestimated efficiency compared with numerical analysis. Snyder and Ursell reported that Eq. **1** works well when the compatibility factor has insignificant variation (32), but it is not enough to show how large the disagreement is in other cases. However, the efficiency difference by Eq. **2** and the numerical simulation is mainly caused by the presence of the Thomson effect that can be informed by $\hat{\alpha}$. In Fig. 4*E*, MgAgSb has $\hat{\alpha}$ below 1, which results in the overrated efficiency by Eq. **2**, and the rest of them have $\hat{\alpha} > 1$ leading to the underrated efficiency compared with the numerical results. Even though the magnitude of $\hat{\alpha}$ does not indicate the exact degree of the error, the intensity of $\hat{\alpha}$ is enough to compare relatively the effect of the Thomson heat among other materials. Fig. 4*F* shows the ΔT-dependent $(PF)_{eng}$, which has the same tendency as the output power density (Fig. 4*F*, *Inset*) under the same leg dimensions. This trend cannot be inferred directly by the conventional *PF*, which only points to the momentary characteristic at a temperature like *ZT*.

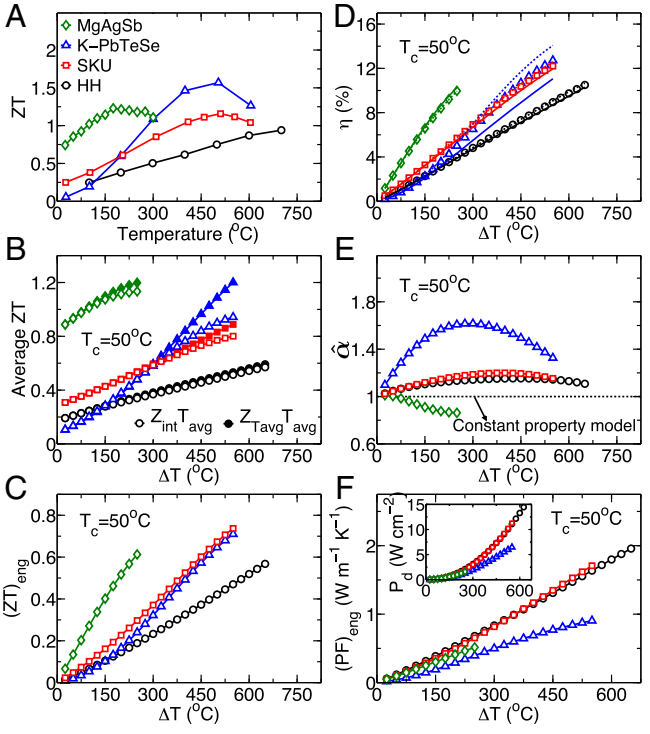

Fig. 4. Effect of the new formulas $(ZT)_{eng}$ and $(PF)_{eng}$, based on cumulative temperature-dependent properties of p-type TE materials. (*A*) Temperature-dependent *ZT*. (*B*) Average *ZT*s by $Z_{int}T_{avg}$(open symbols) and $Z_{T_{avg}}T_{avg}$(solid symbols). (*C*) $(ZT)_{eng}$. (*D*) Efficiency predicted by simulation (open symbols), Eq. **1** (dashed lines), and Eq. **2** (solid lines). (*E*) ΔT-dependent $\hat{\alpha}$. (*F*) ΔT-dependent $(PF)_{eng}$, and power density (*Inset*). The cold-side temperature is fixed as $T_c = 50$ °C for all analysis (*B*)–(*F*) on MgAgSb (26), K-PbTeSe (21), SKU (14), and HH (13).

Generic Formula for Maximum Efficiency Including Thomson Heat. As discussed, the Thomson effect is missing in the evaluation of heat flux by Eq. **2**, which may cause under- or overestimation of the efficiency depending on the degree of Thomson heat at a given temperature gradient. Some studies evaluated the conversion efficiency analytically accounting for the Thomson effect, but they are valid only in limited conditions by assuming a constant Thomson coefficient (29, 33), linear behavior of *S*, ρ, and κ (34), and a temperature-dependent Seebeck coefficient with constant ρ and κ (35). In this section, a generic formula including Thomson heat is established to account for temperature dependence of *S*, ρ, κ, and τ at a large temperature difference, where τ is the Thomson coefficient, and no assumption is required to specify the type of temperature dependence of *S*, ρ, κ, and τ. In addition, practical fractions of Joule and Thomson heat returning to the hot end are evaluated by defining weight factors W_J and W_T, respectively.

The governing equation for energy balance over one-dimensional heat flow is (7)

$$\frac{d}{dx}\left(\kappa(T)\frac{dT}{dx}\right)+J^2\rho(T)-J\tau(T)\frac{dT}{dx}=0, \qquad [5]$$

where *x* and *J* are the distance from the heat source and current density, respectively, and $\tau(T)$ is the temperature-dependent Thomson coefficient defined as $\tau(T) = TdS(T)/dT$. By integrating Eq. **5** twice with respect to *x* and applying the boundary conditions of $T|_{x=0} = T_h$ and $T|_{x=L} = T_c$, where *L* is a length of the TE leg, the input heat Q_h at the hot side becomes

$$Q_h=\frac{A}{L}\int_{T_c}^{T_h}\kappa(T)dT+IT_hS(T_h)-W_JI^2R-W_TI\int_{T_c}^{T_h}\tau(T)dT, \qquad [6]$$

where *A* and *I* are the cross-sectional area and electric current, respectively. W_J and W_T are defined as dimensionless weight factors of Joule and Thomson heat, respectively,

$$W_J=\frac{\int_{T_c}^{T_h}\int_{T}^{T_h}\rho(T)dTdT}{\Delta T\int_{T_c}^{T_h}\rho(T)dT} \text{ and } W_T=\frac{\int_{T_c}^{T_h}\int_{T}^{T_h}\tau(T)dTdT}{\Delta T\int_{T_c}^{T_h}\tau(T)dT}, \qquad [7]$$

where a linear temperature distribution in the TE leg is assumed, i.e., $dT/dx \approx -\Delta T/L$. W_J and W_T lead to practical contributions of Joule and Thomson heat to the heat flux rather than the lumped fraction of 1/2 to the hot and cold side based on the constant property model (7). The conversion efficiency accounting for the Thomson effect, the ratio of output power to input heat rate, is finalized as (see *SI Derivation of the Maximum Efficiency Including Thomson Heat* for a detailed derivation)

$$\eta_{max}=\eta_c\frac{\sqrt{1+(ZT)_{eng}\alpha_1\eta_c^{-1}}-1}{\alpha_0\sqrt{1+(ZT)_{eng}\alpha_1\eta_c^{-1}}+\alpha_2}, \qquad [8]$$

where

$$\alpha_i = \frac{S(T_h)\Delta T}{\int_{T_c}^{T_h} S(T)dT} - \frac{\int_{T_c}^{T_h} \tau(T)dT}{\int_{T_c}^{T_h} S(T)dT} W_T\eta_c - iW_J\eta_c. \quad [9]$$

Eq. **8** is a generic expression that can be transformed into the conventional maximum efficiency formula, Eq. **1**. When the constant property model is considered, i.e., $W_J = 1/2$, $Z_{eng} = Z$ (Z_{int} or $Z_{T_{avg}}$), and $\tau = 0$, Eq. **8** yields Eq. **1**. In addition, by only taking $W_J = 1/2$ and $\tau = 0$ to take $(ZT)_{eng}$ without the Thomson effect on heat flux into consideration, Eq. **8** also becomes Eq. **2**. Thus, the formulas in this section are generic expressions for maximum efficiency, which can be unrestrictedly applied to any case regardless of the temperature dependence of S, ρ, κ, and τ.

Fig. 5*A* shows the maximum efficiency prediction of K-PbTeSe and SnSe according to a temperature gradient by ramping T_h up to each material's limit temperature while $T_c = 50$ °C, where the solid line indicates the maximum efficiency predicted by a numerical simulation. Fig. 5*B* shows how relatively accurate the efficiency calculations are compared with the efficiency η_n by the numerical simulation. The calculation by Eq. **1** overestimates the efficiency by 10% of relative difference for K-PbTeSe at $T_h =$ 600 °C and more than twofold for SnSe at $T_h = 700$ °C compared with the numerical prediction. The maximum efficiency by Eq. **2** reduces the difference, but still overestimates by 17% of relative difference for SnSe, whereas K-PbTeSe is underestimated at a similar degree of relative difference from Eq. **1**. On the other hand, the maximum efficiency by Eq. **8** is predicted more accurately by 5% and 9% of relative difference for K-PbTeSe and SnSe, respectively, which results from taking not only the effect of $(ZT)_{eng}$ but also the Thomson effect into account. Fig. 5 *C* and *D* shows the calculated efficiencies and their accuracy with respect to η_n of HH and SKU, in which the calculated efficiencies of both materials by the three efficiency formulas have good agreement within 4% of relative difference compared with those by numerical simulation. The relatively accurate efficiency and small variation of the prediction for HH and SKU compared with K-PbTeSe and SnSe is caused by the linear-like behavior of their S, ρ, and κ with low rate of change with respect to temperature. Even though Eq. **1** for HH shows better agreement with the numerical results than Eq. **2**, this result is by chance due to offsetting the effects of temperature dependence of S, ρ, and κ according to the assumption of the constant property model, so it

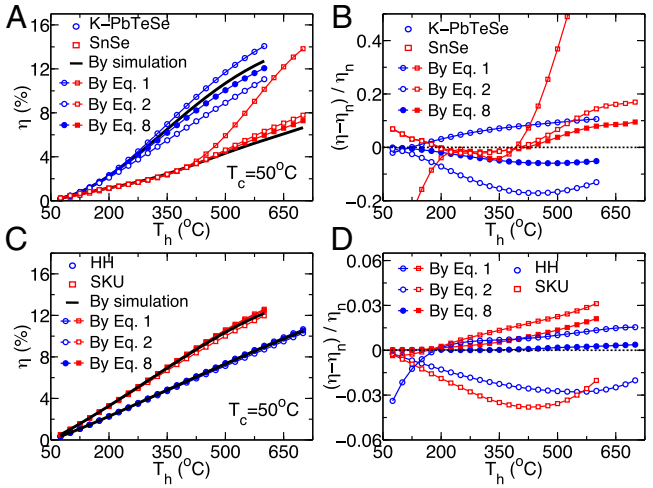

Fig. 5. Effect of the generic formulas for the maximum efficiency. (*A*) Predicted efficiencies as a function of ΔT and (*B*) relative accuracy with respect to numerical results of K-PbTeSe (21) and SnSe (22). (*C*) Predicted efficiency and (*D*) relative accuracy of HH (13) and SKU (14).

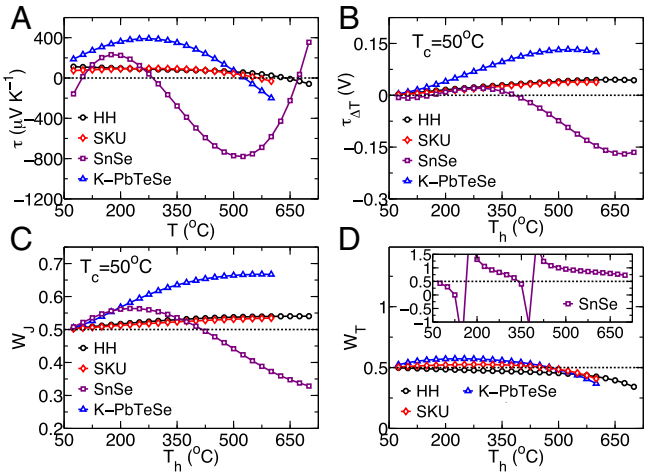

Fig. 6. Contribution for accurate efficiency prediction by overall Thomson coefficient and weight factors. (*A*) Calculated Thomson coefficient τ at each temperature, and (*B*) the overall Thomson coefficient $\tau_{\Delta T}$ as a function of T_h at $T_c = 50$ °C. ΔT-dependent weight factor for (*C*) Joule heating W_J, and (*D*) Thomson heating W_T, where T_c is fixed at 50 °C.

is difficult to analytically predict which material gives rise to the fortuitous type of accurate result by Eq. **1**. However, Eq. **8** leads to the most accurate efficiency predictions by the lowest percentages of relative difference—by 5.1% for K-PbTeSe and by 9.5% for SnSe (Fig. 5*B*), and by 0.4% for HH and by 2% for SKU (Fig. 5*D*)—resulting from the accounting for cumulative temperature dependence, Thomson effect, and modified intensity of Joule and Thomson heating on the hot side.

The further improvement by Eq. **8** compared with Eq. **2** is associated with the temperature-dependent $\tau(T)$ representing the intensity of Thomson heat (Fig. 6*A*). The positive τ implying $dS/dT > 0$ contributes to increasing the efficiency compared with $\tau = 0$ (29), where τ indicates the intensity of the Thomson effect at each temperature. To examine the ΔT-dependent Thomson heating at a large temperature difference, the overall Thomson coefficient at given T_h and T_c, defined as $\tau_{\Delta T} = \int_{T_c}^{T_h} \tau(T)dT$, is shown in Fig. 6*B*, where positive values of $\tau_{\Delta T}$ for K-PbTeSe, HH, and SKU over the whole temperature range lead to increasing the efficiency compared with that by Eq. **2**, so it is closer to the efficiency predicted by numerical analysis. The overall effect of Thomson heating associated with ΔT for SnSe differs in temperature boundaries where $\tau_{\Delta T}$ fluctuates across zero. $\tau_{\Delta T}$ at 150 °C $< T_h <$ 400 °C is positive, so that Eq. **2** underestimates the efficiency more so than Eq. **8**, whereas negative $\tau_{\Delta T}$ above $T_h =$ 400 °C gives rise to the overestimated efficiency (Fig. 5 *A* and *B*). Thus, Eq. **8** can indicate whether the efficiency is over- or underrated compared with that by Eq. **2**. However, the efficiency results from the interrelation of conduction and Joule and Thomson heat, as well as the temperature dependence of S, ρ, and κ, so it is difficult to exactly predict the quantified degree of accuracy between Eq. **8** and the numerical simulations. The reasons for the inaccuracy are the linearized expression of dT/dx, and the different type of temperature dependence, i.e., cumulative in this study and instantaneous in the numerical model.

Fig. 6 *C* and *D* shows ΔT-dependent weight factors for Joule and Thomson heating, respectively, based on the analysis by the cumulative temperature-dependent properties. In Fig. 6*C*, W_J of SnSe fluctuates across 1/2 (by the constant property model) while the others monotonically increase over 1/2 with T_h. The increasing W_J at larger ΔT indicates that a larger fraction of Joule heating returns to the hot side than 1/2 of it due to their increasing trend of $\rho(T)$. ΔT-dependent W_T is shown in Fig. 6*D*, where W_T for K-PbTeSe, HH, and SKU have decreasing tendencies and become below 1/2 at certain T_h, which means the effect by Thomson heat on the heat flux at the hot end gets

smaller because their dS/dT decreases. For SnSe, ΔT-dependent W_T (Fig. 6*D*, *Inset*) has two diverged points around 150 °C and 400 °C at which $\tau_{\Delta T}$ becomes zero (Fig. 6*B*), indicating that no overall Thomson heating through a material at the temperature difference is considered even though Thomson heating exists at each temperature. W_T in Eq. **7** becomes infinite when $\tau_{\Delta T} = 0$, which seems to make Eq. **9** invalid, but it does not affect the efficiency analysis because W_T is always paired with $\tau_{\Delta T}$. Thomson heat influences back to the hot sides of HH, SKU, K-PbTeSe, and SnSe are 20.6%, 33.9%, 55.3%, and −17.3% of Joule heat, respectively, where the negative sign indicates the opposite direction of Joule heat. Because Thomson and Joule heating are electric current dependent, the relative percentage is estimated at the current flow through a cubic-shaped leg ($1 \times 1 \times 1$ mm^3).

Conclusions

We found the unreliability of using ZT to predict efficiency by the conventional efficiency formula that has been commonly used since the 1950s, so we defined $(ZT)_{eng}$ and $(PF)_{eng}$ for the realistic evaluation of a TE material's efficiency and output power, respectively, associated with any practical temperature difference between the cold and hot sides. Based on $(ZT)_{eng}$, the new efficiency formula was derived, where the degree of Thomson effect can be identified analytically by $\hat{\alpha}$ enabling one to predict the relative difference of efficiency compared with numerical simulations, even though the formula does not consider the Thomson effect on heat flux evaluation. To supplement the absence of Thomson heat, we also established a formula including Thomson heat by defining the overall Thomson effect $\tau_{\Delta T}$ through a given temperature difference. This is generic and can be simply converted to the models by constant properties (Eq. **1**) as well as cumulative temperature-dependent properties excluding the Thomson effect (Eq. **2**). The ΔT-dependent weight factors lead to practical contributions of Joule and Thomson heat to the heat flux at hot side at a given temperature difference rather than the concept of returning half of them each to the hot and cold sides regardless of boundary temperatures. Therefore, our new efficiency formulas should be used for reliable evaluation of the maximum efficiency of any TE materials. $(PF)_{eng}$ correctly indicates the intrinsic characteristics for output power generation of thermoelectric materials, and $(ZT)_{eng}$ is a practical indicator to correctly show the practical efficiency under any temperature difference unlike the average ZTs from the conventional ZT curves. We expect these new formulas will have a profound impact on the search for new materials, the design of devices, and the studies of systems for the energy community.

ACKNOWLEDGMENTS. This work was partially supported by the US Department of Energy (DOE) under Contract DOE DE-FG02-13ER46917/DE-SC0010831 (the part without the Thomson effect) and also partially by Solid State Solar Thermal Energy Conversion Center (S^3TEC), an Energy Frontier Research Center funded by the US DOE, Office of Science, Office of Basic Energy Science under Award DE-SC0001299 (the part considering the Thomson effect). The work is also supported in part by US Air Force Office of Scientific Research Grant FA9550-09-1-0656, the T. L. L. Temple Foundation, the John J. and Rebecca Moores Endowment, and the State of Texas through the Texas Center for Superconductivity at the University of Houston.

1. Rowe DM (1995) *CRC Handbook of Thermoelectrics* (CRC, Boca Raton, FL).
2. Bell LE (2008) Cooling, heating, generating power, and recovering waste heat with thermoelectric systems. *Science* 321(5895):1457–1461.
3. Zebarjadi M, Esfarjani K, Dresselhaus MS, Ren ZF, Chen G (2012) Perspectives on thermoelectrics: From fundamentals to device applications. *Energy Environ. Sci.* 5(1): 5147–5162.
4. Liu W, Jie Q, Kim HS, Ren ZF (2015) Current progress and future challenges in thermoelectric power generation: From materials to devices. *Acta Mater* 87:357–376.
5. Altenkirch E (1909) Uber den Nutzeffekt der Thermosaulen. *Phys Z* 10:560–568.
6. Ioffe AF (1957) *Semiconductor Thermoelements and Thermoelectric Cooling* (Infosearch, London).
7. Angrist SW (1965) *Direct Energy Conversion* (Allyn and Bacon, Boston).
8. Goldsmid HJ, Sheard AR, Wright DA (1958) The performance of bismuth telluride thermojunctions. *Br J Appl Phys* 9(9):365–370.
9. Snyder GJ, Toberer ES (2008) Complex thermoelectric materials. *Nat Mater* 7(2):105–114.
10. Lan Y, Minnich AJ, Chen G, Ren ZF (2010) Enhancement of thermoelectric figure-of-merit by a bulk nanostructuring approach. *Adv Funct Mater* 20(3):357–376.
11. Poudel B, et al. (2008) High-thermoelectric performance of nanostructured bismuth antimony telluride bulk alloys. *Science* 320(5876):634–638.
12. Wu HJ, et al. (2014) Broad temperature plateau for thermoelectric figure of merit ZT>2 in phase-separated $PbTe_{0.7}S_{0.3}$. *Nat Commun* 5:4515.
13. He R, et al. (2014) Investigating the thermoelectric properties of p-type half-Heusler $Hf_x(ZrTi)_{1-x}CoSb_{0.8}Sn_{0.2}$ by reducing Hf concentration for power generation. *RSC Adv.* 4(110):64711–64716.
14. Jie Q, et al. (2013) Fast phase formation of double-filled p-type skutterudites by ball-milling and hot-pressing. *Phys Chem Chem Phys* 15(18):6809–6816.
15. Shuai J, et al. (2015) Study on thermoelectric performance by Na doping in nanostructured $Mg_{1-x}Na_xAg_{0.97}Sb_{0.99}$. *Nano Energy* 11:640–646.
16. Hsu KF, et al. (2004) Cubic $AgPb_mSbTe_{2+m}$: bulk thermoelectric materials with high figure of merit. *Science* 303(5659):818–821.
17. Rhyee J-S, et al. (2009) Peierls distortion as a route to high thermoelectric performance in $In_4Se_{3-\delta}$ crystals. *Nature* 459(7249):965–968.
18. Bhame SD, Pravarthana D, Prellier W, Noudem JG (2013) Enhanced thermoelectric performance in spark plasma textured bulk n-type $BiTe_{2.7}Se_{0.3}$ and p-type $Bi_{0.5}Sb_{1.5}Te_3$. *Appl Phys Lett* 102(21):211901.
19. Kim HS, Kikuchi K, Itoh T, Iida T, Taya M (2014) Design of segmented thermoelectric generator based on cost-effective and light-weight thermoelectric alloys. *Mater Sci Eng B* 185:45–52.
20. Koirala M, et al. (2013) Thermoelectric property enhancement by Cu nanoparticles in nanostructured $FeSb_2$. *Appl Phys Lett* 102(21):213111.
21. Zhang Q, et al. (2012) Heavy doping and band engineering by potassium to improve the thermoelectric figure of merit in p-type PbTe, PbSe, and $PbTe_{1-y}Se_y$. *J Am Chem Soc* 134(24):10031–10038.
22. Zhao L-D, et al. (2014) Ultralow thermal conductivity and high thermoelectric figure of merit in SnSe crystals. *Nature* 508(7496):373–377.
23. Liu W, et al. (2015) n-type thermoelectric material $Mg_2Sn_{0.75}Ge_{0.25}$ for high power generation. *Proc Natl Acad Sci USA* 112(11):3269–3274.
24. Liu W, et al. (2013) Studies on the Bi_2Te_3-Bi_2Se_3-Bi_2S_3 system for mid-temperature thermoelectric energy conversion. *Energy Environ. Sci.* 6(2):552–560.
25. Zhang Q, et al. (2015) Enhancement of thermoelectric performance of n-type PbSe by Cr doping with optimized carrier concentration. *Adv Energy Mater* 5(8):1401977.
26. Kraemer D, et al. (2015) High thermoelectric conversion efficiency of MgAgSb-based material with hot-pressed contacts. *Energy Environ Sci* 8(4):1299–1308.
27. Hogan TP, Shih T (2005) *Thermoelectrics Handbook: Macro to Nano* (Taylor & Francis, Boca Raton, FL).
28. Mahan GD (1991) Inhomogeneous thermoelectrics. *J Appl Phys* 70(8):4551–4554.
29. Sunderland JE, Burak NT (1964) The influence of the Thomson effect on the performance of a thermoelectric power generator. *Solid-State Electron* 7(6): 465–471.
30. Müller E, Zabrocki K, Goupil C, Snyder G, Seifert W (2012) Functionally graded thermoelectric generator and cooler elements. *CRC Handbook of Thermoelectrics: Thermoelectrics and Its Energy Harvesting*, ed Rowe DM (Taylor & Francis, Boca Raton, FL), Vol 1.
31. Muto A, Kraemer D, Hao Q, Ren ZF, Chen G (2009) Thermoelectric properties and efficiency measurements under large temperature differences. *Rev Sci Instrum* 80(9): 093901.
32. Snyder GJ, Ursell TS (2003) Thermoelectric efficiency and compatibility. *Phys Rev Lett* 91(14):148301.
33. Min G, Rowe DM, Kontostavlakis K (2004) Thermoelectric figure-of-merit under large temperature differences. *J Phys D Appl Phys* 37(8):1301–1304.
34. Yamashita O (2008) Effect of linear temperature dependence of thermoelectric properties on energy conversion efficiency. *Energy Convers Manage* 49(11): 3163–3169.
35. Chen J, Yan Z, Wu L (1996) The influence of Thomson effect on the maximum power output and maximum efficiency of a thermoelectric generator. *J Appl Phys* 79(11): 8823–8828.